International Journal of Control, Automation, and Systems (2009) 7(1):75-84 http://www.springer.com/12555
DOI 10.1007/s12555-009-0110-2

Balance Control of a Biped Robot Using Camera Image of Reference Object

Sangbum Park, Youngjoon Han, and Hernsoo Hahn

Abstract: This paper presents a new balance control scheme for a biped robot. Instead of using dynamic sensors to measure the pose of a biped robot, this paper uses only the visual information of a specific reference object in the workspace. The zero moment point (ZMP) of the biped robot can be calculated from the robot's pose, which is measured from the reference object image acquired by a CCD camera on the robot's head. For balance control of the biped robot a servo controller uses an error between the reference ZMP and the current ZMP, estimated by Kalman filter. The efficiency of the proposed algorithm has been proven by the experiments performed on both flat and uneven floors with unknown thin obstacles.

Keywords: Balance control, biped robot, reference object image, zero moment point.

1. INTRODUCTION

Vision sensor has been generally used for path planning and for obstacle avoidance in walking robots. However, visual information can be used very effectively for maintaining balance of a walking robot. It can be proven by the fact that a human may experience difficulty in walking straight with eyes closed. This phenomenon shows that humans not only depend on the vestibular organ, but also significantly on the information acquired by visual system to keep the balance of body while walking. With this analogy, biped robots simulating the human body may use a vision sensor to control and thus maintain the balance of body while walking.

Nowadays, applications of visual information for motion control can be easily found in industrial robots. Such applications are mostly concentrated on visual servoing of manipulators which controls the pose of end-effecter to approach a specific trajectory by measuring the target trajectory using the visual information [1-3]. Since visual servoing is used to control a manipulator based on analysis of images being provided in real-time, the problem of accurately extracting the 3D pose of the reference coordinate system with less computational time becomes the major issue. To reduce the computational complexity required for solving this problem, Chesi [4] proposed a method of using 6 instead of 8 feature points which have been required for the traditional visual servoing techniques to extract the 3D pose of the reference object. It was made possible by calculating the geometrical relations among the feature points to reduce the number of variables. Radu [5] proposed a method of aligning the pose of the first manipulator (where a camera is mounted on its end-effecter) to the pose of the second manipulator using the visual information provided by the camera. The pose of the first manipulator is estimated from the image feature points of the second manipulator's gripper.

There are also few other examples that have applied visual servoing techniques for balance control of biped robots. Different from the visual servoing techniques used for the manipulators whose base frame is fixed to the ground, but those which are used in biped robots, should consider the fact that the center of mass (COM) or the zero moment point (ZMP) of robot is not static while a robot is walking. For the control of a biped robot using visual information, the relationship between the camera pose and the ZMP of the robot should be updated repetitively. In order to apply the visual servoing technique used for manipulator having 6 degrees of freedom to the positioning control of a biped robot, Yamamura [6] fixed the geometrical relation between the camera frame and the robot frame to reduce the degree of freedom of each leg to 4. This approach of adapting a visual servoing technique for manipulator to the one for biped robot limits the robot's locomotion significantly.

To solve the aforementioned problems involved in using visual information for balance control, this paper proposes a new balance control method for the biped robot. For this purpose, initially the motion structure of a biped robot is approximated using 3D-LIPM (3D-Linear Inverted Pendulum Mode) scheme and the reference ZMP trajectory of a biped robot is generated. The pose of the biped robot with respect to the reference object is measured from the input image acquired by a CCD camera fixed on the head of the robot. Since the biped robot is structured so as to have the COM coincided with

Manuscript received May 14, 2007; revised February 5, 2008 and June 18, 2008; accepted September 29, 2008. Recommended by Editorial Board member Dong Hwan Kim under the direction of Editor Jae-Bok Song. This work was supported by the Korea Research Foundation Grant funded by the Korean Government (MOEHRD). This research was supported by the MKE(The Ministry of Knowledge Economy), Korea, under the ITRC (Information Technology Research Center) support program supervised by the IITA(Institute for Information Technology Advancement) (IITA-2008-C1090-0803-0006).

Sangbum Park, Youngjoon Han, and Hernsoo Hahn are with the School of Electronic Engineering, Hyungnam Memorial Bd., Soongsil University, 511 Sangdo-dong, Dongjak-gu, Seoul, 156-743 Korea (e-mails: {forcepsb, young, hahn}@ssu.ac.kr).

© ICROS, KIEE and Springer 2009

the center of the pelvis, the biped robot has little magnitude of error in the position difference between them [7,8] which may be ignored. Therefore, the COM of the biped robot can be calculated from its pose. For the balance control of the biped robot, the servo controller uses the error between the reference ZMP trajectory and the current ZMP estimated by Kalman filter.

The rest of this paper is organized as follows. In Section 2, the structural characteristics and the walking patterns of the biped robot based on 3D-LIPM are illustrated. In Section 3, the camera model is given, and the pose of the robot with respect to the object frame is measured from the reference object image acquired by the camera. The relationship between the pose and COM is also explained in this Section. In Section 4, the balance control scheme is described, which uses the error between the reference ZMP trajectory and the current ZMP estimated by Kalman filter, as an input to the PID controller. The performance of the proposed balance control scheme is evaluated by the experiments described in Section 5.

2. STRUCTURAL CHARACTERISTICS OF THE BIPED ROBOT

In this section, firstly, the structural characteristics of the biped robot used in this paper are illustrated. Afterwards, the walking pattern generation scheme is illustrated which simplifies the structural model of the robot as an inverse pendulum using the 3D-LIPM scheme and generates the symmetric and periodic walking patterns.

2.1. Structure of the biped robot

Each leg of the biped robot has 6 degrees of freedom so that the foot may generate any pose in 3D space as shown in Fig. 1(a).

For simplifying the kinematics analysis, the number of DH (Denavit-Hartenberg) parameters is reduced by aligning the ankle joint and the pelvis joint axes. The robot has no joint in the waist to align the upper body and the camera axis and each arm has 3 degrees of freedom as shown in Fig. 1(b).

2.2. Structure of the biped robot

Biped robot requires complex dynamic modeling and analysis processes to analyze a simple symmetric and

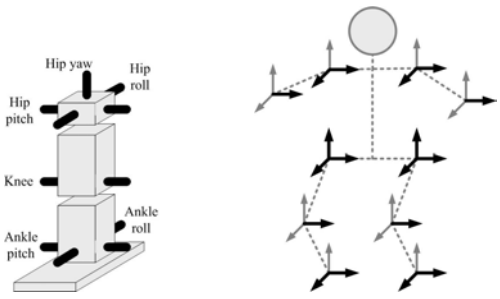

(a) Joints in the leg. (b) Joints in the biped robot.

Fig. 1. Distribution of joints in the biped robot.

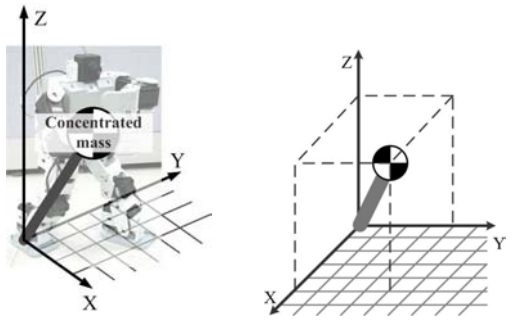

Fig. 2. Motion representation of the biped robot using the 3D-LIPM.

periodic walking motion of a leg having six degrees of freedom. Although several processes are used, it is not guaranteed that the robot's motion can be exactly analyzed. Thus as many other researches have used earlier, this paper also uses the 3D-LIPM scheme to approximate the motion of the biped robot as that of the inverse pendulum as shown Fig. 2. The pendulum is the mass point which represents the most dominant motion of the biped robot [9,10].

One important feature of human walking is that the height of pelvis changes little. This feature helps to simplify the complex dynamic equation by limiting the height of the motion of mass point in 3D-LIPM to a specific plane. By the analysis of the dynamics of the 3D-LIPM scheme, the relation between the COM and ZMP can be represented by the following equations [7].

$$-\frac{z_c}{g}\ddot{x}+x=P_x,\quad -\frac{z_c}{g}\ddot{y}+y=P_y. \tag{1}$$

In (1), (x, y) and $(\ddot{x}, \ddot{y})$ are the differential and acceleration of the COM in a biped robot in X and Y axes respectively, g is the gravity acceleration, (P_x, P_y) are ZMP in (X, Y) plane, and z_c is the height of the COM which does not change while the robot moves.

The principle of dynamic walking [11], guides that a biped robot may walk stable as long as the projection of the ZMP of the robot on the floor points to the contacted region in the feet. From this principle, the trajectory of

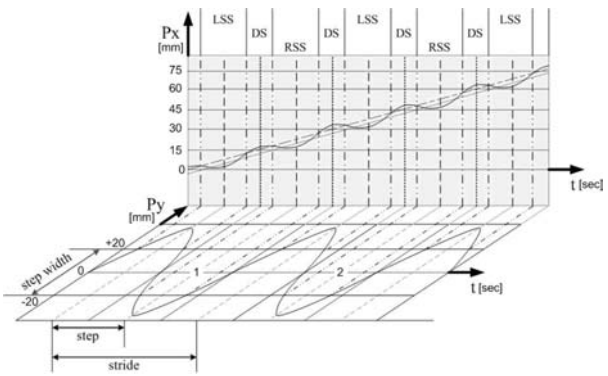

Fig. 3. ZMP trajectory of biped robot approximated as a sine wave form.

ZMP that the robot should satisfy for stable walking can be constructed from the trajectory of the feet. Fig. 3 shows an example of ZMP trajectory having a form of sine wave generated considering the symmetry and periodicity of the trajectory of the feet. As shown below, LSS(Left Single Side), DS(Double Side), RSS(Right Single Side) are included as the state of robot.

To determine the y axis value of the COM first, the trajectory of P_y having the angular velocity ω_y is represented as follows:

$$P_y = A\sin\omega_y t. \tag{2}$$

By applying (2), equation (1) is represented as the canonical non-homogeneous 2nd order differential equation as follows.

$$\ddot{y} - \frac{g}{z_c} y = -\frac{g}{z_c} A\sin\omega_y t. \tag{3}$$

Since the force function P_y in the above equation is a sine wave, the steady state solution y will also be represented as a function of the sine waves whose angular velocity is ω_y.

$$y = A_1\cos\omega_y t + B_1\sin\omega_y t. \tag{4}$$

By applying this function to Eq. (4) and solving the equation with respect to y, Eq. (5) is obtained as the steady state solution.

$$y = \frac{g}{z_c\omega_y^2 + g}\cdot P_y \tag{5}$$

The x trajectory of ZMP is designed for the biped robot to have the lower speed in order to decrease the moment of inertia when the robot foot is touched on the floor. In addition, the biped robot has the highest speed at the instance when the ZMP of the biped robot points into the double support area. As shown in Fig. 3, the force function P_x has the sine wave with the double angle velocity ($2\omega_y$) of P_y, and the average velocity of the biped robot according to x coordinate is the slope of the P_x function respect to time coordinate. The trajectory of P_x having the angular velocity ω_x is represented as follows:

$$P_x = \Theta_\theta[A\sin\omega_x t]. \tag{6}$$

where, the operator Θ_θ expresses the rotation of θ with respect to time coordinate. The x position of COM can be determined as follows:

$$x = \Theta_\theta\left[\frac{g}{z_c\omega_x^2 + g}\cdot P_x\right]. \tag{7}$$

Equations (5) and (7) show that the coordinates of COM is linearly proportional to the coordinates of ZMP when the motion of COM of the biped robot is restricted to a plane where $Z=z_c$ and the trajectory of ZMP is approximated as a sine wave.

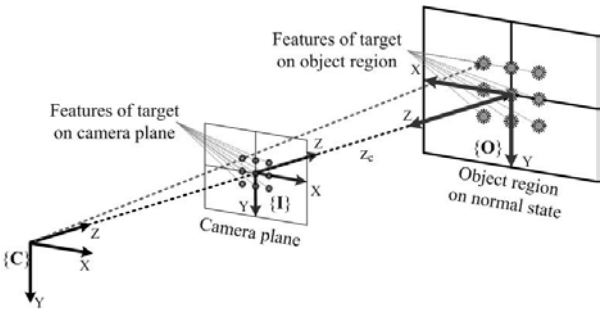

Fig. 4. Pin-hole camera model to project ${}^c\mathbf{P}_i$ on the image frame.

3. ESTIMATION OF ROBOT POSE FROM THE POSE OF THE REFERENCE OBJECT IN INPUT IMAGE

For simplifying the process of determining the pose of the camera with respect to the reference object, it is assumed that the feature points of the reference object are located on the same plane. This paper uses the reference object which has nine feature points equally spaced on the same plane, as shown in Fig. 4. Each feature point ${}^o\mathbf{P}_i$ is represented by the homogeneous vector in the reference object frame, {**O**}, as given in Eq. (8), and it is viewed as ${}^o\mathbf{P}_i$ in the camera frame, {**C**}, as given in (9).

$${}^o\mathbf{P}_i = ({}^oX_i, {}^oY_i, {}^oZ_i, 1), \qquad (i = \{1,2,\cdots,9\}) \tag{8}$$

$${}^c\mathbf{P}_i = {}^c\mathbf{H}_o\,{}^o\mathbf{P}_i,$$

$${}^c\mathbf{H}_o = \begin{bmatrix}\mathbf{R} & \mathbf{T}\\ \mathbf{0} & \mathbf{1}\end{bmatrix} = \begin{bmatrix}R_{11} & R_{12} & R_{13} & T_x\\ R_{21} & R_{22} & R_{23} & T_y\\ R_{31} & R_{32} & R_{33} & T_z\\ 0 & 0 & 0 & 1\end{bmatrix}. \tag{9}$$

In the homogeneous matrix ${}^c\mathbf{H}_o$ in (9), **R** is a rotational matrix and **T** is the translation vector. In the image frame, {**I**}, each feature point ${}^c\mathbf{P}_i$ in the camera frame is represented by the 2D vector whose coordinates are obtained by a perspective projection of the point using the pin-hole camera model, as shown in Fig. 4. Then the projected feature point in the image frame is represented by $\mathbf{p}_i=(x_i,y_i,1)$.

The perspective projection using the pin-hole camera model projects a 3D point ${}^c\mathbf{P}_i=({}^cX_i, {}^cY_i, {}^cZ_i, 1)$ in the camera frame onto $\mathbf{p}_i=(x_i,y_i,1)$ in the image frame, using the following transformation matrix given in (10).

$$\begin{bmatrix}x_i\\ y_i\\ 1\end{bmatrix} = \frac{1}{{}^cz_i}\begin{bmatrix}f & 0 & 0 & 0\\ 0 & f & 0 & 0\\ 0 & 0 & 1 & 0\end{bmatrix}\begin{bmatrix}{}^cX_i\\ {}^cY_i\\ {}^cZ_i\\ 1\end{bmatrix}. \tag{10}$$

Thus, the target is to extract the feature point ${}^c\mathbf{P}_i=({}^cX_i, {}^cY_i, {}^cZ_i, 1)$ in the camera frame inversely from measured feature point $\mathbf{p}_i=(x_i,y_i,1)$ in the image frame, and then

derive ${}^{c}\mathbf{H}_{o}$ using the interrelationships among different correspondences ${}^{c}\mathbf{P}_{i}$ and ${}^{o}\mathbf{P}_{i}$. To derive ${}^{c}\mathbf{P}_{i}$ from $\mathbf{p}_{i}$ in the image, $\mathbf{p}_{i}$ should be represented using the internal variables in the computer image space using (11).

$$\begin{bmatrix} u_i \\ v_i \\ 1 \end{bmatrix} = \begin{bmatrix} f \cdot s_x & f \cdot s_\theta & u_0 \\ 0 & f \cdot s_y & v_0 \\ 0 & 0 & 1 \end{bmatrix} \begin{bmatrix} x_i \\ y_i \\ 1 \end{bmatrix}. \tag{11}$$

In (11), s_x and s_y are given as the horizontal and vertical sizes of an image pixel respectively. $f \cdot s_\theta$ is the skew of a pixel whose value is near zero, and (u_0, v_0) is the coordinates of a point in the computer image space, such that the optical axis of the camera lens is projected in the image plane. Since the distortion caused by the camera lens can be calibrated by the algorithm described in [12], the lens distortion variables are not considered in this paper and the skew is ignored.

Since the feature points are located in the X-Y plane in the object frame as shown in Fig. 4, their Z coordinate are zero and they can be represented as ${}^{c}\mathbf{P}_{i}=({}^{c}\mathrm{X}_{i}, {}^{c}\mathrm{Y}_{i}, {}^{c}\mathrm{Z}_{i}, 1)$,(i=1…9). These points are represented as (u_i, v_i) in the computer image space and to derive inversely ${}^{c}\mathbf{P}_{i}$ from (u_i, v_i) the following parallel (12) is calculated from (9)-(11).

$$\begin{aligned} f \cdot s_x \cdot {}^{o}X_i \frac{R_{11}}{T_z} + f \cdot s_x \cdot {}^{o}Y_i \frac{R_{12}}{T_z} - (u_i - u_0) \cdot {}^{o}X_i \frac{R_{31}}{T_z} \\ - (u_i - u_0) \cdot {}^{o}Y_i \frac{R_{32}}{T_z} + f \cdot s_x \frac{T_x}{T_z} = u_i - u_0, \\ f \cdot s_y \cdot {}^{o}X_i \frac{R_{21}}{T_z} + f \cdot s_y \cdot {}^{o}Y_i \frac{R_{22}}{T_z} - (v_i - v_0) \cdot {}^{o}X_i \frac{R_{31}}{T_z} \\ - (v_i - v_0) \cdot {}^{o}Y_i \frac{R_{32}}{T_z} + f \cdot s_y \frac{T_y}{T_z} = v_i - v_0. \end{aligned} \tag{12}$$

By inserting the coordinates of the nine feature points in the object frame as in (12), (13) is obtained which includes all the components of ${}^{c}\mathbf{H}_{o}$, and the goal matrix is further derived as in (14).

$$\mathbf{AK} = \mathbf{B} \tag{13}$$

$$\mathbf{A} = \begin{bmatrix} fs_x {}^{o}X_1 & fs_x {}^{o}Y_1 & 0 & 0 & -(u_1-u_0){}^{o}X_1 & -(u_1-u_0){}^{o}Y_1 & fs_x & 0 \\ 0 & 0 & fs_y {}^{o}X_1 & fs_y {}^{o}Y_1 & -(v_1-v_0){}^{o}X_1 & -(v_1-v_0){}^{o}Y_1 & 0 & fs_y \\ fs_x {}^{o}X_2 & fs_x {}^{o}Y_2 & 0 & 0 & -(u_2-u_0){}^{o}X_2 & -(u_2-u_0){}^{o}Y_2 & fs_x & 0 \\ 0 & 0 & fs_y {}^{o}X_2 & fs_y {}^{o}Y_2 & -(v_2-v_0){}^{o}X_2 & -(v_2-v_0){}^{o}Y_2 & 0 & fs_y \\ \vdots & \vdots & \vdots & \vdots & \vdots & \vdots & \vdots & \vdots \\ fs_x {}^{o}X_9 & fs_x {}^{o}Y_9 & 0 & 0 & -(u_9-u_0){}^{o}X_9 & -(u_1-u_0){}^{o}Y_9 & fs_x & 0 \\ 0 & 0 & fs_y {}^{o}X_9 & fs_y {}^{o}Y_9 & -(v_9-v_0){}^{o}X_9 & -(v_1-v_0){}^{o}Y_9 & 0 & fs_y \end{bmatrix}$$

$$\mathbf{K} = \begin{bmatrix} \frac{R_{11}}{T_z} & \frac{R_{12}}{T_z} & \frac{R_{21}}{T_z} & \frac{R_{22}}{T_z} & \frac{R_{31}}{T_z} & \frac{R_{32}}{T_z} & \frac{T_x}{T_z} & \frac{T_y}{T_z} \end{bmatrix}^T$$

$$\mathbf{B} = \begin{bmatrix} u_1 - u_o & v_1 - v_o & u_2 - u_o & v_2 - v_o & \cdots & u_9 - u_o & v_9 - v_o \end{bmatrix}^T.$$

Equation (13) shows that the coordinates of at least 4 feature points should be measured exactly to derive **K**. In other words, it means that 4 feature points are sufficient to derive ${}^{c}\mathbf{H}_{o}$ if all 4 points can be measured. Since there is a possibility of false detection of the feature points due to noise in input image, this paper uses the reference object having 9 feature points, and the coordinates of the feature points measured in the image frame are applied to Eq. (14) to find **K** using a least mean square method.

$$\mathbf{K} = (\mathbf{A}^T \mathbf{A})^{-1} \mathbf{A}^T \mathbf{B}. \tag{14}$$

To calculate T_z in **K** we use the property of the rotational matrix, that the column vectors are orthogonal and also the condition that T_z is much larger than f.

$$T_z = f + \frac{1}{2}\left(\frac{1}{\sqrt{K_1^2 + K_3^2 + K_5^2}} + \frac{1}{\sqrt{K_2^2 + K_4^2 + K_6^2}} \right). \tag{15}$$

In (15), K_i is the i-th elements of vector **K** (in (13)). The solution of T_z is acquired from the average of the two calculated values, and the homogeneous transformation matrix ${}^{c}\mathbf{H}_{o}$ between the camera frame and the object frame which can be calculated by it. As shown in Fig. 6, the homogeneous matrix ${}^{c}\mathbf{H}_{o}$ can determine the robot's pose relative to the object frame.

4. BALANCE CONTROL USING CAMERA POSE

As shown in Fig. 5, the camera frame is fixed on the top of the biped robot so that the robot frame can be automatically determined once the pose of the camera is measured. Thus, the balance control of the biped robot becomes a problem of determining the stable pose of the robot while walking.

For generating the stable walking pattern of the robot, this paper uses the ZMP trajectory as explained in Section 2, which calculates the COM trajectory. As the biped robot Cycloid is used for our task, it is structured so as to have the COM coincided with the center of the pelvis, the biped robot has a small amount of error in the position difference between them [7,8] that may be ignored. Therefore, the COM of the biped robot can be represented by (16) from the transformation relationship among the frames defined in Fig. 6.

$$\mathbf{H}_m = \mathbf{H}_o ({}^{m}\mathbf{H}_c \, {}^{c}\mathbf{H}_o)^{-1} = \mathbf{H}_o \, {}^{o}\mathbf{H}_c \, {}^{c}\mathbf{H}_m. \tag{16}$$

Since the COM measured from the reference object image could contain noises, the ZMP of the robot which is calculated by (5) and (6) may be different from the

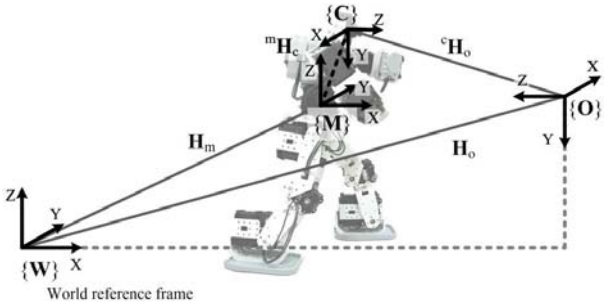

Fig. 5. The relationships among the frames defined in the working environment.

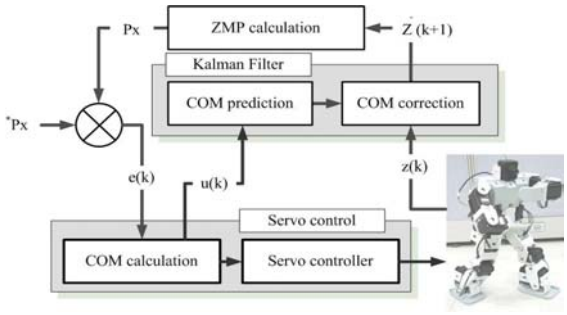

Fig. 6. Balance control of Biped Robot using Kalman filter.

reference ZMP trajectory. And the balance control of the biped robot has the general problem that it uses the error signal between the reference ZMP and the current measured ZMP as the next period control signal. As shown in Fig. 6, this paper estimates the current ZMP using Kalman filter and uses the feedback system with error signal (**e**(*k*)) which is occurred in the reference ZMP trajectory [10].

First, the error signal **e**(*k*) is transferred to a PID controller. The error signal **e**(*k*) on ZMP space is transformed into an error signal on COM space, and the error signal on COM space is transferred both to PID controller's input and the Kalman filter's input simultaneously. The PID controller derives velocities of individual joints to control the robot from the error signal. The Kalman filter estimates the COM using the error signal input and the system noise. The COM correction in Kalman filter is performed from the measured pose of the biped robot and the measurement noise. The current of ZMP can be calculated by applying the corrected points shown in (5) and (7).

For the balance control of the biped robot, the system equation of the Kalman filter which consists of the feedback system is given in (17):

$$\hat{\mathbf{x}}(k) = \mathbf{A}\hat{\mathbf{x}}(k-1) + \mathbf{B}\mathbf{u}(k) + \mathbf{w}(k-1), \tag{17}$$

$$\mathbf{x}(k) = \begin{bmatrix} x & y & \dot{x} & \dot{y} & \ddot{x} & \ddot{y} \end{bmatrix}^T,$$

$$\mathbf{A} = \begin{bmatrix} 1 & 0 & \Delta t & 0 & \Delta t^2 & 0 \\ 0 & 1 & 0 & \Delta t & 0 & \Delta t^2 \\ 0 & 0 & 1 & 0 & \Delta t & 0 \\ 0 & 0 & 0 & 1 & 0 & \Delta t \\ 0 & 0 & 0 & 0 & 1 & 0 \\ 0 & 0 & 0 & 0 & 0 & 1 \end{bmatrix},$$

$$\mathbf{w}(k) : \mathbf{N}(0, \mathbf{Q}_1),$$

where the 6×1 state vector **x**(*k*) consists of position, velocity, and acceleration of the COG and the 6×6 matrix **A** is the state transition matrix which transforms the current state to the next state. The product of the input matrix **B** and the input **u**(*k*) is provided as the external input value to the Kalman filter. The 6×1 vector **w**(*k*) is the system state error, which has the property of a zero-mean white Gaussian noise.

If the relation between the system state and the measured value is linear, the measurement equation is given in (18).

$$\hat{\mathbf{z}}(k) = \mathbf{H}\mathbf{x}(k) + \mathbf{v}(k), \tag{18}$$

$$\mathbf{z}(k) = \begin{bmatrix} x_{com} & y_{com} \end{bmatrix}^T,$$

$$\mathbf{H} = \begin{bmatrix} 1 & 0 & \Delta t & 0 & \Delta t^2 & 0 \\ 0 & 1 & 0 & \Delta t & 0 & \Delta t^2 \end{bmatrix},$$

$$\mathbf{v}(k) \approx \mathbf{N}(0, \mathbf{Q}_2),$$

where the 2×1 measurement vector **z**(*k*) is the pose of the robot which is calculated from the image information. The 2×6 measurement matrix **H** expresses the relation between the system state and the measurement vector. In addition, the measurement error **v**(*k*) has the property of zero-mean, white Gaussian noise with $\mathbf{Q}_2$ covariance.

The Kalman filter estimates a process state by using a form of feedback control: time update equations and measurement update equations. The time update equations are responsible for projecting forward (in time) the current state and error covariance estimates to obtain the a priori estimates for the next time step. The measurement update equations are responsible for the feedback—i.e., for incorporating a new measurement into the a priori estimate to obtain an improved a posteriori estimate.

The time update equations are given in (19) and (20).

$$\hat{\mathbf{x}}(k)^- = \mathbf{A}\hat{\mathbf{x}}(k-1) + \mathbf{B}\mathbf{u}(k), \tag{19}$$

$$\mathbf{P}(k)^- = \mathbf{A}\mathbf{P}(k-1)\mathbf{A}^T + \mathbf{Q}, \tag{20}$$

where **P**(*k*) and **P**(*k*)$^-$ are a posteriori estimate error covariance and priori estimate error covariance, respectively.

And the measurement update equations are given as following

$$\mathbf{K}(k) = \mathbf{P}(k)\mathbf{H}^T(\mathbf{H}\mathbf{P}(k)^-\mathbf{H}^T + \mathbf{R})^{-1}, \tag{21}$$

$$\mathbf{x}(k)^- = \hat{\mathbf{x}}(k)^- + \mathbf{K}(k)(\mathbf{z}(k) - \mathbf{H}\hat{\mathbf{x}}(k)^-), \tag{22}$$

$$\mathbf{P}(k) = (\mathbf{I} - \mathbf{K}(k)\mathbf{H})\mathbf{P}(k)^-, \tag{23}$$

where the difference $\mathbf{z}(k) - \mathbf{H}\hat{\mathbf{x}}(k)^-$ in (22) is called the measurement innovation. It reflects the discrepancy between the predicted measurement and the actual measurement.

The first task during the measurement update is to compute the Kalman gain, **K**(*k*). The next step is to actually measure the process to obtain **z**(*k*), and then to generate an a posteriori state estimate by incorporating the measurement as in (22). The final step is to obtain an a posteriori error covariance estimate via (23). After each time and measurement update pair, the process is repeated with the previous a posteriori estimates used to project or predict the new a priori estimates.

The robust control of the biped robot can be archived by estimating the current ZMP using the Kalman filter. But the stable servo control must be designed to stabilize the biped robot. This paper designs the PID controller

that has good control properties. The PID output $\mathbf{u}_{\mathbf{PID}}(k)$ for controlling velocities of individual joints is given in (24):

$$\mathbf{u}_{PID}(k) = K_p\mathbf{e}(k) + \mathbf{K}_I \sum_{n=0}^{k} \mathbf{e}(n) + K_d(\mathbf{e}(k) - \mathbf{e}(k-1)), \quad (24)$$

where K_p, K_I, and K_d are the proportional gain, the integral gain, and the derivative gain respectively. This PID controller gain is manually tuned to adjust to the response of the whole system.

5. EXPERIMENTS

The performance of the proposed scheme has been evaluated with the biped robot Cycloid, manufactured by Robotize Cooperation whose structural characteristics are explained in Section 2. The CCD camera with image sensor size is 300×220 pixels and frame rate is 25 [fps] is mounted on the robot head. The object frame {**O**} was located at (1100mm, 0mm, 360mm) with (-90deg, 90deg, 0deg) rotated relative to the world frame. The reference object is consisting of red dots equally spaced on a white plane and their centers are used as the feature points.

To visualize the process of the proposed algorithm, a GUI composed of three modules has been implemented.

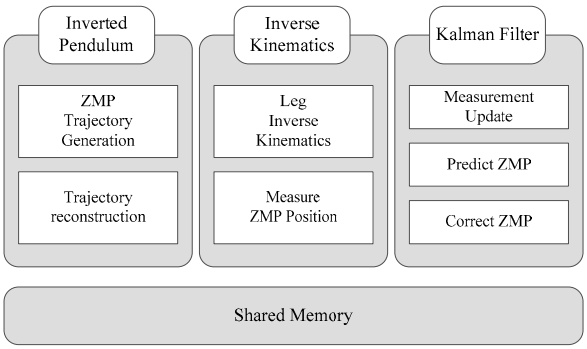

(a) Block diagram of the proposed algorithm.

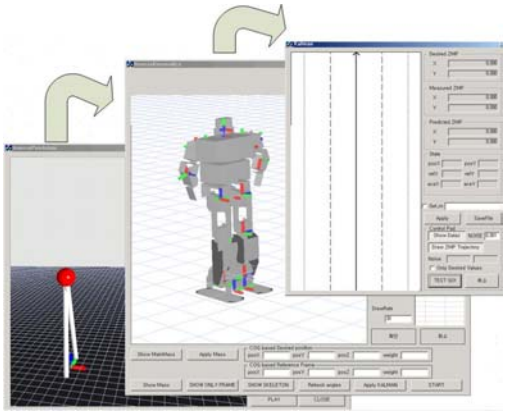

(b) GUI showing the process of the proposed algorithm.

Fig. 7. GUI for visualizing the experimental process.

The first one is to show the reference trajectory represented by that of COM of the biped robot using the 3D-LIPM. The second one shows how the Kalman filter estimates the ZMP state in the next step from the current COM of the robot which is measured from the reference object image. The third one shows how closely the actual robot trajectory follows the reference trajectory one.

This GUI of the robot is developed using OpenGL graphics modules based on the kinematics information. The three modules are connected by the shared memory as shown in Fig. 7(a) and the process of the proposed algorithm is illustrated graphically as shown in Fig. 7(b).

In this section, earlier to testing the proposed algorithm, the characteristics of error included in the ZMP measurement of the biped robot acquired from the reference image is analyzed, and then the performance of the proposed balance control scheme is explained. The experiments have been performed under two different floor conditions, 1) a flat floor without obstacle, and 2) an uneven floor with thin obstacles of 5mm height.

5.1. Measurement of the camera pose from a reference object image

In order to measure the pose of the biped robot from a reference image, the pose of camera frame has to be measured first. The precision of the measured pose of a camera frame is largely affected by image noise and camera lens distortion. To acquire the statistical characteristics of the measurement error, the distance and orientation of the reference object are measured repetitively using the camera located at the head of the robot and the average and variance of the measurements errors are calculated. Initially the camera frame was located at (0mm, 0mm, 360mm) and rotated by (-90deg, 90deg, 0deg) with reference to the world frame. The orientation was measured with rotating the lens axis about the individual axes by 15deg from -30deg to +30deg, and the distance was measured with moving by 15mm each step from a distance of 1250mm toward the reference object along the X axis as shown in Fig. 8.

Table 1 summarizes the average and variance error measurements included in the orientation and distance measurements. The average and variance of the rotation measurement errors are 0.36deg and 2.01deg^2 respectively. In Table 1(a), the error occurring in case of rolling appears smaller than those occurring in the other cases, since the rotation is about the optical axes and thus there

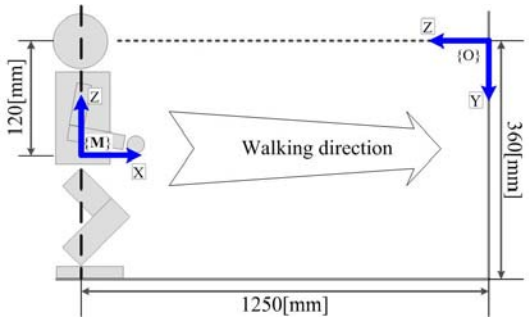

Fig. 8. Orientation and distance measurement for extracting the error characteristics.

Table 1. Error characteristics included in the orientation and distance measurements.

(a) Error included in the orientation measurement.

Roatation axis and angle[deg]		Average [deg]	Variance [deg]
Rolling	+30	0.28	1.43
	+15	0.36	1.59
	-15	0.24	1.59
	-30	0.40	1.75
Pitching	+30	0.35	2.20
	+15	0.21	1.77
	-15	0.33	1.80
	-30	0.38	1.95
Yawing	+30	0.43	2.89
	+15	0.46	2.14
	-15	0.49	2.43
	-30	0.53	3.35
No rotation		0.20	1.25
Average		0.36	2.01

(b) Error included in the distance measurement.

Distance from the reference object [mm]	Average [mm]	Variance [mm]
950	5.35	10.36
1000	5.25	11.38
1050	3.51	9.02
1100	4.01	8.43
1150	3.61	8.19
1200	4.97	11.44
1250	4.68	13.07
Average	4.49	10.27

is no distortion included. The average and variance of the distance measurement errors are 4.49mm and 10.27mm^2 respectively. These statistical error charac-teristics are used in the Kalman filter to estimate the ZMP of the robot in the following experiments.

5.2. Robot walking on a flat floor with no obstacle

For balance control of biped robot, the proposed algorithm uses an error between the desired ZMP and the estimated ZMP by Kalman filter as the input of the PID controller. The robot initially located at (0mm, 0mm, 240mm) in the world frame walked towards the reference object along the X axis of the robot frame which coincides with the Z axis of the reference object frame. The performance of the balance control algorithm is tested by measuring how accurately the robot follows the desired ZMP trajectory. Fig. 9 shows four trajectories, acquired when the robot walk with an optimal speed of 20mm/sec. The first is the ZMP trajectory obtained by only PID controller, the second one is obtained by PID controller based on Kalman Filter, and the third is the error signal between the desired ZMP trajectory and the

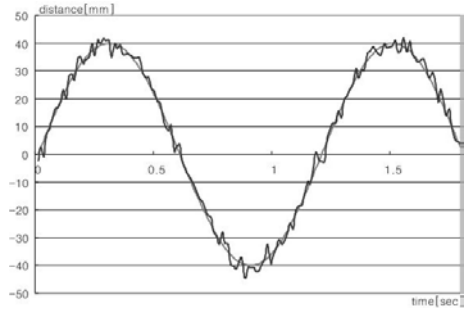

(a) The acquired ZMP trajectory using only PID controller.

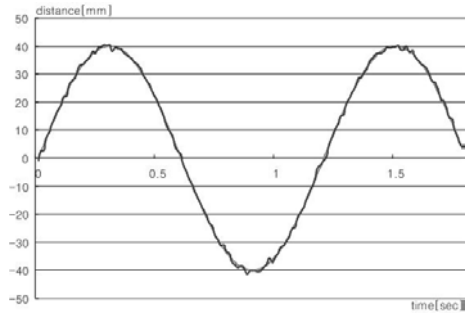

(b) The acquired ZMP trajectory using PID controller based on Kalman filter.

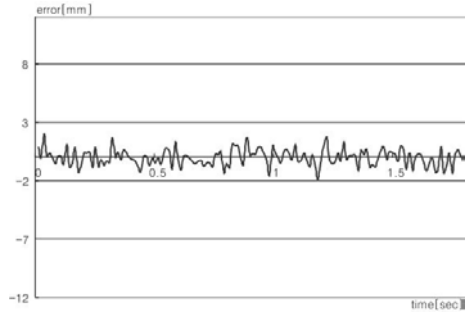

(c) Error in (b).

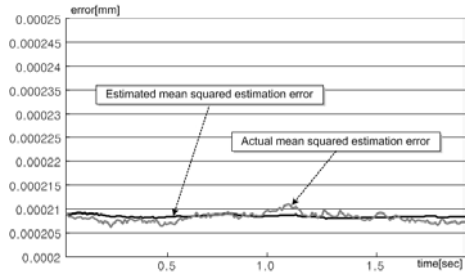

(d) The estimated mean square estimation error and the actual mean square estimation error in (c).

Fig. 9. Acquired ZMP trajectories using the proposed algorithm are compared with the reference trajectory when the robot walks with the speed of 20mm/sec.

actual ZMP trajectory shown in Fig. 9(b). The perfor-mance of the proposed Kalman filter is shown in Fig. 9(d). It plots the estimated mean squared estimation error of the ZMP trajectory against the actual mean squared

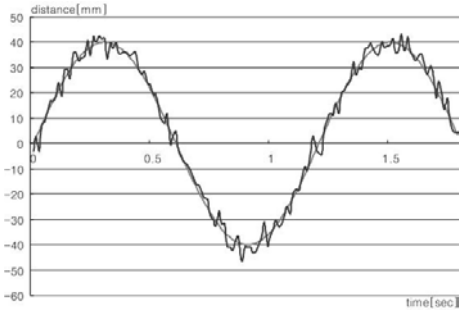

(a) The acquired ZMP trajectory using only PID controller.

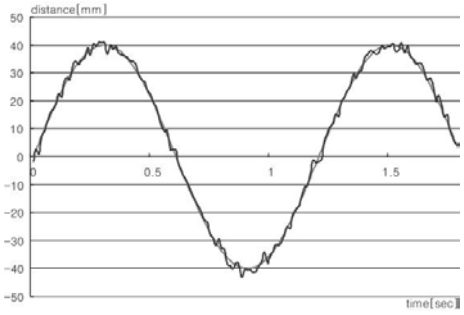

(b) The acquired ZMP trajectory using PID controller based on Kalman filter.

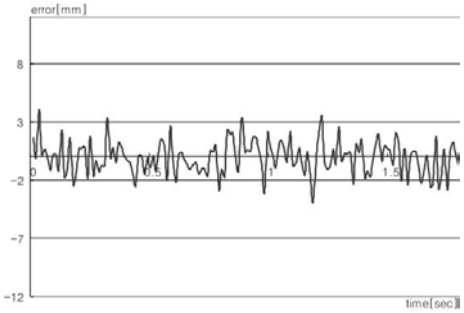

(c) Error in (b).

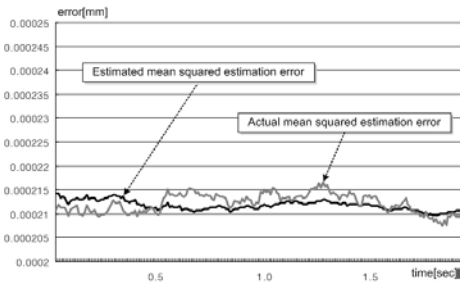

(d) The estimated mean square estimation error and the actual mean square estimation error in (c).

Fig. 10. Acquired ZMP trajectories using the proposed algorithm are compared with the reference values when the robot walks with the speed of 40mm/sec.

estimation error of the ZMP trajectory in Fig. 9(c).

The estimated mean squared estimation error is induced by (5) and (7) from the first and second diagonal elements of the error covariance matrix P(k). It can be seen that the Kalman Filter estimates the actual trajectory accurately and with estimation can be trusted to maintain stability.

The experimental results have shown that the balance control using only camera is successful since the robot follows the desired ZMP trajectory within a reasonably small error boundary. The average error was 1.73mm while using only a PID controller and it was 0.57mm when using the Kalman filter based on PID controller.

Since the accuracy of balance control can be affected by the periodic time of commands along with the walking speed, the algorithm was tested while robot walking with the maximum speed of 40[mm/sec]. This can be achieved by adjusting the periodic time of commands, which is represented as the sum of image processing and servo control times as given in (21).

$$\begin{aligned}&\text{Command period(50ms)} = \\ &\text{Image processing(40ms)} + \text{Servo control(10ms)}\end{aligned} \tag{21}$$

The maximum periodic time of commands (cycle) is 50ms(20Hz) was empirically determined on the condition that the frame rate of the camera is 30fps. At the maximum periodic time of command, the walking speed of the robot becomes 40mm/sec. Experimental results acquired when the robot walked with the maximum speed, are illustrated in Fig. 10.

As expected, the measurement errors increased to twice of those acquired when the robot walks at the optimal speed. The average errors are displayed as shown in Fig. 10. The ZMP error of the proposed servo control with respect to Y axis was 1.15mm, but the general servo control had the ZMP error of 2.31mm.

5.3. Robot walking on an uneven floor with unknown thin obstacle

To see how the robot responds when facing unexpected walking environment, an uneven floor was artificially constructed by locating the flat bars on the floor arbitrarily, as shown in Fig. 11. Each bar has a thickness of 2mm. It was programmed in such a way that the robot may put a step on the stick when the biped robot reaches a stable state.

The ZMP trajectories acquired using the PID controller and the Kalman filter based PID controller illustrated in Fig. 12 where they are compared to the desired trajectory. As shown in Fig. 12, the obstacles affect the balance of the robot but their consequences are very quickly recovered. Fig. 12(a) shows that the disturbance caused by the obstacles has a large magnitude (18.82mm on average) but they disappears in 7 periodic time of commands on average, when using only the PID controller. In the similar situation, Fig. 12(b) shows that the disturbance has a smaller magnitude (14.92mm on average) and also disappears in 4 periodic time of commands on average, which is two times faster than the case shown in Fig. 12 by using the Kalman filter based PID controller.

Fig. 11. Robot walks on an uneven floor with unknown thin obstacle.

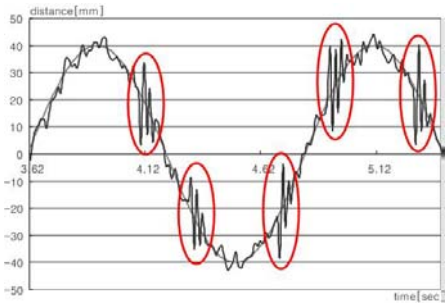

(a) ZMP trajectory acquired using the PID controller.

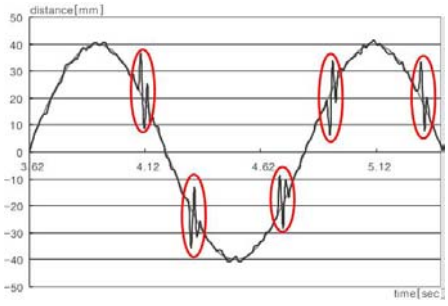

(b) ZMP trajectory acquired using the Kalman filter based PID controller.

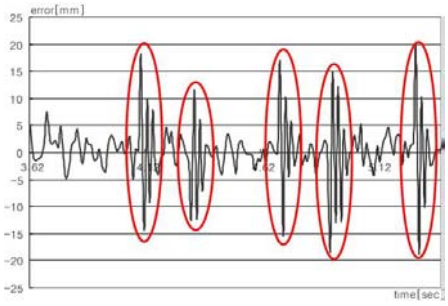

(c) Error in (a).

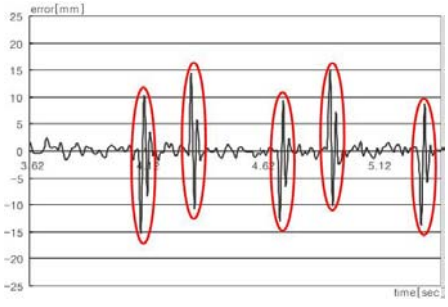

(d) Error in (b).

Fig. 12. Acquired ZMP trajectories when the robot walks on an uneven floor.

6. CONCLUSION

This paper proposed a new balance control scheme for a biped robot, which uses the visual information of a specific reference object in the workspace to measure the ZMP of the robot. The pose of biped robot is thus determined without using any dynamic sensor. The pose of the robot at each sampling time was determined using a PID controller, so that the current ZMP of the robot may be located at the desired ZMP positioned inside the stable region of the robot. The experimental results have shown that the ZMP trajectory generated by the PID controller, whose current ZMP is determined only using the visual information, follows the desired trajectory very closely. It is also shown by the experiments that the performance of the PID controller could be enhanced significantly when the ZMP of the robot is estimated using the Kalman filter. The biped robot could maintain the balance on both flat and uneven floors using the proposed algorithm.

REFERENCES

[1] W. Yu, "Stability analysis of visual servoing with sliding-mode estimation and neural compensation," *International Journal of Control, Automation, and Systems*, vol. 4, no. 5, pp. 545-558, 2006.

[2] C. Taylor and J .Ostrowski, "Robust vision-based pose control," *Proc. of IEEE International Conference on Robotics and Automation*, pp. 2734-2740, 2000.

[3] C. Cho, S. Kang, M. Kim, and J.-B. Song, "Macro-micro manipulation with visual tracking and its application to wheel assembly," *International Journal of Control, Automation, and System*, vol. 3, no. 3, pp. 461-468, 2005.

[4] G. Chesi and K. Hashimoto, "Camera pose estimation from less than eight points in visual servoing," *Proc. of IEEE International Conference on Robotics and Automation*, vol. 1, pp. 733-738, 2004.

[5] R. P. Horaud, F. Dornaika, C. Laugier, and C. Bard, "Integrating grasp planning and visual servoing for automatic grasping," *Experimental Robotics IV:4th International Symposium*, vol. 223, pp.71-82,1997.

[6] Y. Yamamura and N. Maru, "Positioning control of the leg of the humanoid robot by linear visual servoing," *Humanoid Robots*, *4th IEEE/RAS International Conference*, vol. 1, pp. 1-12, 2004.

[7] K. Nishiwaki, S. Kagami, Y. Kuniyoshi, M. Inaba, and H. Inoue, "online generation of humanoid walking motion based on a fast generation method of motion pattern that follows desired zmp," *Proc. of IEEE/RSJ International Conference on Intelligent Robots and Systems*, vol. 3, pp. 2684-2689, 2002.

[8] K. Sorao, T. Murakami, and K.Ohnishi, "A unified approach to zmp and gravity center control in biped dynamic stable walking," *Proc. of Advanced Intelligent Mechatronics*, 1997.

[9] T. Sugihara, Y. Nakamura, and H. Inoue, "Realtime humanoid motion generation through zmp manipu-

lation based on inverted pendulum control," *Proc. of IEEE International Conference on Robotics and Automation*, pp. 1404-1409, 2002.
[10] S. Kajita, F. Kanehiro, K. Kaneko, K. Fujiwara, K. Harada, K. Yokoi, and H. Hirukawa, "Biped walking pattern generation by using preview control of zero-moment point," *Proc. of IEEE International Conference on Robotics and Automation*, pp. 1620-1626, 2003.
[11] K. Sorao, T. Murakami, and K. Ohnishi, "A unified approach to ZMP and gravity center control in biped dynamic stable walking," *Proc. of Advanced Intelligent Mechatronics*, 1997.
[12] H. Tang, L. Wang, and Z. Sun, "Accurate and stable vision in robot soccer," *Proc. of Control, Automation, Robotics and Vision Conference*, vol. 3, pp. 2314-2319, 2004.

Sangbum Park received the B.S. and M.S. degrees from Electronic Engineering of Soongsil University, Seoul, Korea, in 2004 and 2006 respectively. He has been with School of Electronic Engineering, Soongsil University since 2006, where he is currently pursuing a Ph.D. His current research interests include biped walking robot, robotics vision.

Youngjoon Han received the B.S., M.S. and Ph.D. degrees in Electronic Engineering from Soongsil University, Seoul, Korea, in 1996, 1998, and 2003, respectively. He is currently an Assistant Professor in the School of Electornic Engineering at Soongsil University. His research interests include robot vision system, and visual servo control.

Hernsoo Hahn received the B.S. and M.S. degrees in Electronic Engineering at Soongsil University and Younsei University, Korea in 1982 and 1983 respectively. He received the Ph.D. degree in Computer Engineering from University of Southern California in 1991, and became an Assistant Professor at the School Electroncis Engneering in Soongsil University in 1992. Currently, he is a Professor. His research interests include application of vision sensors to mobile robots and measurement systems.